https://doi.org/10.5194/egusphere-2025-6569
Preprint. Discussion started: 16 February 2026

Case Studies on Mesospheric Fronts at Low Latitudes over Brazil

Efua Ogobor[1], Igo Paulino[2], Vania F. Andrioli[3], Cristiano M. Wrasse[4], Hisao Takahashi[3], Amauri F. Medeiros[2], Paulo P. Batista[3], Prosper K. Nyassor[4]

[1]National Space Research and Development Agency, Abuja, Nigeria.
[2]Unidade Acadêmica de Física, Universidade Federal de Campina Grande, Campina Grande, PB, Brazil.
[3]Divisão de Heliofísica, Ciências Planetárias e Aeronomia, Instituto Nacional de Pesquisas Espaciais, São José dos Campos, SP, Brazil
[4]Divisão de Clima Espacial, Instituto Nacional de Pesquisas Espaciais, São José dos Campos, SP, Brazil.

Correspondence to: Prosper K. Nyassor (prosper.nyassor@inpe.br)

Abstract. This study investigates four mesospheric front events observed over Cachoeira Paulista (23°S, 45°W), Brazil, between 2007 and 2008, using coordinated measurements from an all-sky airglow imager, meteor wind radar, and sodium temperature lidar. The events, recorded on 14–15 September 2007, 5 October 2007, 31 March 2008, and 3 September 2008, were classified as mesospheric bores, two undular and two turbulent based on airglow morphology and atmospheric background structure. Vertical profiles of wind and temperature, along with vertical wavenumber diagnostics, revealed the presence of thermal and thermal-Doppler ducts supporting the bores. Classical complementary emission responses were observed in single-duct environments, while multi-duct layering led to complex airglow signatures, including mixed bright and dark fronts. This is the first study in Brazil's low-latitude region to employ simultaneous multi-instrument observations for mesospheric bore analysis, offering new insights into duct dynamics, emission behavior, and wave–duct interactions in the mesosphere and lower thermosphere.

1 Introduction

Mesospheric fronts are dynamic atmospheric phenomena occurring in the mesosphere and lower thermosphere (MLT) region, often associated with the propagation and breaking of gravity waves. These fronts, observable as sharp airglow boundaries in all-sky images, play a crucial role in understanding vertical atmospheric coupling and energy transfer processes at low and mid-latitudes. Depending on their morphology and generation mechanisms, mesospheric fronts are generally classified into three types: (i) undular bore fronts, (ii) turbulent bore fronts, and (iii) wall fronts (Dewan & Picard, 1998; Smith et al., 2005). Undular bore fronts are typically supported by vertical ducting in the MLT region, resulting from thermal inversions, Doppler shifts, or a combination of both (thermal-Doppler ducts). Their distinguishing feature is the presence of trailing wave trains behind the leading front. Turbulent bores, although also duct-supported, lack these trailing

https://doi.org/10.5194/egusphere-2025-6569
Preprint. Discussion started: 16 February 2026

waves and instead exhibit signs of nonlinear dissipation behind the front. Wall fronts, in contrast, arise from freely propagating gravity waves that become unstable and break in a non-ducted atmosphere. Although wall fronts may mimic bore morphology in airglow images, they differ fundamentally in origin.

The initial observation and characterization of mesospheric bore events emerged from the ALOHA-93 campaign (Taylor et al., 1995), which reported sharp wavefronts in OH, Na, O_2, and OI 557.7 nm airglow emissions. Subsequent studies (e.g., Smith et al., 2005; Medeiros et al., 2005; Narayanan et al., 2009; Fechine et al., 2009; Medeiros et al., 2018) refined this classification based on trailing wave behavior, duct structure, and emission intensity. Ducting mechanisms such as thermal inversions, wind shear, or their combination i.e., thermal-Doppler ducts, determine whether gravity waves steepen into bores or dissipate. The so-called complementary effect, proposed by Dewan and Picard (1998), describes how the duct's placement relative to airglow layers can produce contrasting intensity changes above and below the duct region.

In recent years, progress has been made in both observing and simulating bore dynamics and ducting conditions. For example, Ramachandran et al. (2023) used numerical simulations and airglow imagery to demonstrate how duct thickness and initial wave amplitude govern bore formation and trailing wave patterns. Hecht et al. (2023) observed a mesospheric bore with high spatial resolution and showed that its dissipation via small-scale instabilities led to momentum flux divergence and mean wind acceleration within a thermal–Doppler duct. Similarly, Simkhada et al. (2008) presented observational evidence of short-period gravity waves and mesospheric bores Doppler ducted in the 80–100 km region, confirming strong wave trapping through matched airglow and wind measurements. A bore–front interaction observed by Mondal et al. (2021) revealed a thermally ducted undular mesospheric bore over the western Himalayas, with its formation attributed to gravity wave–duct interactions and its dissipation linked to neutral instabilities and weakening of the duct layer.

In the South American sector, recent climatological and case studies have improved understanding of low-latitude gravity wave dynamics. Carvalho et al. (2023) analyzed 10 years of mesospheric front activity over São João do Cariri (7.4°S), identifying a strong seasonal pattern and preferential north-eastward propagation. In southern Brazil, Li et al. (2025) reported long-lasting, intense concentric gravity waves (CGWs) over southern Brazil linked to fast-moving severe thunderstorms, with multi-instrument observations revealing their propagation from the mesosphere to the thermosphere and highlighting the role of weak background winds and Doppler-shift effects in enabling vertical coupling across atmospheric layers. While Wrasse et al. (2024) analyzed over 200 quasi-monochromatic gravity wave events observed over southern Brazil, attributing their seasonal propagation patterns to background wind dynamics and identifying jet stream–cold front interactions as a key source mechanism through case-specific ray-tracing analysis.

Despite these advances, there remains a shortage of high-resolution, multi-instrument case studies exploring mesospheric front dynamics at low-latitudes in Brazil. This study addresses the gap by analyzing four mesospheric front events observed over Cachoeira Paulista (23°S, 45°W) between 2007 and 2008, using coordinated measurements from an all-sky airglow imager, an interferometric meteor radar, and a sodium (Na) temperature lidar. These four events were classified as mesospheric bores, comprising two undular and two turbulent cases. Detailed analysis of background wind and temperature profiles was conducted to characterize ducting conditions (thermal, Doppler, or combined) and to investigate the

https://doi.org/10.5194/egusphere-2025-6569
Preprint. Discussion started: 16 February 2026

presence of the complementary effect across different airglow layers. This work not only contributes to one of the few simultaneous observational studies of mesospheric fronts in Brazil but also contextualizes these events within the broader theoretical and observational frameworks developed in recent years. The findings provide new insights into duct size, duct-induced bore formation and the variability of wave–duct interactions under low-latitude MLT conditions.

2 Instrumentation and Methods

Simultaneous data were acquired using an all-sky airglow imager, an interferometric meteor radar, and a Na temperature lidar over Cachoeira Paulista (23° S, 45° W), Brazil, between 2007 and 2008. Together, these instruments provided high-resolution measurements of airglow structures, horizontal winds, and temperature profiles in the MLT region. The objective was to characterize the morphology and background conditions associated with each front and to identify the nature and source of any ducting mechanisms.

The all-sky airglow imager used in this study is equipped with a back-illuminated CCD camera (1340 × 1300 pixels, 20 µm pixel size), a 180° fish-eye lens, and a telecentric optical system. It includes a filter wheel and objective lens, enabling sequential imaging of key mesospheric airglow emissions: hydroxyl (OH, 715–930 nm), molecular oxygen (O_2, 0–1), and atomic oxygen (OI 557.7 nm). These emissions originate at nominal peak altitudes of approximately 87 km (OH), 94 km (O_2), and 97 km (OI 557.7 nm). Integration times were 15 s for OH and 90 s for both O_2 and OI. Images were on-chip binned to 650 × 670 pixels to enhance the signal-to-noise ratio. Observations were conducted under moonless, clear-sky conditions when the Sun and Moon were at least 12° and 0° below the horizon, respectively. More details about the Cachoeira Paulista all-sky imager have been reported by Medeiros et al. (2004).

Temperature profiles were measured using a narrowband Na temperature lidar located at São José dos Campos (23° S, 46° W), approximately 100 km east of Cachoeira Paulista. This system uses resonant scattering from the mesospheric sodium layer to retrieve temperature profiles between 80 and 100 km altitude, with a vertical resolution of 0.5 km and a temporal resolution of 2.5 minutes. The lidar operates by mixing the outputs of two Nd:YAG lasers (at 1064 nm and 1319 nm) to generate the 589 nm emission needed to probe the Na D2a line. Both lasers are CW-seeded to maintain a spectral linewidth below 100 MHz. Temperatures were calculated by comparing backscattered signals at the Na resonance peak and crossover minimum. The absolute temperature uncertainty is estimated at ±5 K in regions with high sodium density. Additional system specifications are provided in Clemesha et al. (2010) and Yang et al. (2010).

Horizontal wind measurements in the MLT region were obtained using an all-sky interferometric meteor radar operating at 35.24 MHz. The system transmits via a three-element Yagi antenna and receives backscattered signals from meteor trails using five two-element Yagi antennas arranged orthogonally. It operates with a 2 kHz pulse repetition frequency and a 13 µs pulse width. The radar provides zonal and meridional wind profiles over the 80–100 km altitude range, with a vertical resolution of 2 km and a temporal resolution of 1 hour. Detailed descriptions of the radar methodology are available in Hocking et al. (2001) and Batista et al. (2002).

https://doi.org/10.5194/egusphere-2025-6569
Preprint. Discussion started: 16 February 2026

To assess the vertical propagation conditions of the observed wavefronts, the square of vertical wavenumber m^2 using the Taylor–Goldstein dispersion relation was computed, which includes both wind and temperature effects (Nappo, 2002)

$$m^2 = \left[\frac{N^2}{(u-c)^2} - \frac{u''}{(u-c)} - k_h^2\right], \quad (1)$$

where, $k_h = 2\pi/\lambda_h$, is the horizontal wavenumber and λ_h is the horizontal wavelength, c is the phase velocity of the wave, u is the wind velocity in the wave direction, and u'' is the second derivative of u with height (z). $N^2 = \left(\frac{g}{\theta}\frac{\partial\theta}{\partial z}\right)$ is the square of Brunt-Vaisala frequency (buoyancy frequency), θ is the potential temperature, g is the acceleration due to gravity. $N^2/(u-c)^2$ represents the temperature effect while $-u''/(u-c)$ represents the wind.

A wave is considered to be freely propagating if $m^2 > 0$; otherwise, it is evanescent. A duct is identified where a region of positive m² is bounded above and below by regions of negative m², enabling vertical trapping and horizontal propagation of gravity waves. By isolating the contributions of temperature and wind to the total m², we classify ducts as thermal, Doppler, or thermal-Doppler types. Spectral characteristics of the wavefronts were analyzed using the OH airglow images, while the O_2 and OI 557.7 nm emissions were used to examine the vertical extent and intensity patterns, particularly in relation to the complementary effect predicted by Dewan and Picard (1998). This multi-instrumental approach allowed for detailed classification of the mesospheric fronts and a comprehensive analysis of the background atmospheric conditions responsible for their formation and evolution.

3 Results and Discussion

This study analyzes four mesospheric front events observed over Cachoeira Paulista (23° S, 45° W), Brazil, between 2007 and 2008, using 27 nights of coordinated measurements. While TIMED/SABER data are commonly used to characterize mesospheric temperature profiles over Brazil, the Na lidar employed in this study offered higher vertical resolution, allowing finer-scale duct structures to be resolved. Consistent with recommendations by Narayanan et al. (2009), the combined use of Na lidar, meteor radar, and all-sky imaging provided a comprehensive diagnostic framework for mesospheric front events. This comprehensive dataset enabled the identification and detailed examination of four prominent events, which occurred on the nights of: (1) 14–15 September 2007, (2) 5 October 2007, (3) 31 March 2008, and (4) 3 September 2008. Each event was interpreted within the framework of mesospheric front theory, with classification based on airglow morphology and the background atmospheric structure. Specifically, vertical profiles of horizontal wind and temperature, combined with vertical wavenumber diagnostics, were used to determine the type of front and the nature of any supporting atmospheric ducting (thermal, Doppler, or thermal-Doppler).

Due to limitations in image quality and signal-to-noise ratio, only the OH emission band was used for quantitative spectral analysis. The O_2 and OI 557.7 nm emissions, although useful for visual confirmation and for estimating the vertical extent of the observed features, were excluded from the spectral analysis. From the OH images, several key spectral

https://doi.org/10.5194/egusphere-2025-6569
Preprint. Discussion started: 16 February 2026

parameters were extracted. These included the horizontal wavelength (λ_h), defined as the horizontal distance in kilometers between successive wave crests; the wave period (τ), which is the time in minutes required for a complete oscillation of the wave; and the phase speed (c), representing the horizontal propagation speed of the wave phase in meters per second (m/s). The analysis also recorded the emission intensity type, distinguishing between bright fronts, where airglow emission is enhanced, and dark fronts, where emission is reduced relative to the background.

Finally, the propagation direction, expressed as the zenithal azimuth angle (ϕ), was determined as the direction of wave travel in degrees measured clockwise from geographic north at the observation zenith. Together, these parameters provided a quantitative description of the dynamical behavior of each mesospheric front and formed the basis for interpreting their interaction with the surrounding MLT. Table 3.1 summarizes the key characteristics of the observed mesospheric front events. It includes the date of each event, the time interval during which spectral analysis was performed on the traveling wave front, and the horizontal wavelengths of the trailing wave structures, which ranged from 32.7 to 40.9 kilometers. Wave periods were within 9.2 to 38.0 min. In particular, Event 4 displayed the longest period of approximately 38.0 minutes, indicating a low-frequency wave compared to other observations. Phase speeds varied considerably, from 14.7 to 74.3 meters per second. Both bright fronts (BF) and dark fronts (DF) were detected, reflecting differences in the vertical structure of the background atmosphere and the relative position of the duct to the emission layer.

Table 1: Mesospheric front parameters from spectral and airglow imaging analysis.

Event	Emission Layer	Date	Local Time (GMT – 3:00)	λ_h (km)	τ (min)	c (m/s)	Emission Type	ϕ (°)
1	OH	14/09/2007	00:16 – 00:36	32.7	14.8	36.7	BF	116.6
2	OH	05/10/2007	21:00 – 21:43	34.7	10.7	54.0	DF	118.3
3	OH	31/03/2008	21:26 – 22:37	33.5	38.0	14.7	DF	121.6
4	OH	03/09/2008	23:16 – 23:30	40.9	9.2	74.3	BF	28.6

3.1 Event 1: 14–15 September 2007 — Turbulent Bore with Complementary Effect

On the night of 14 –15 September 2007, a mesospheric front was observed over Cachoeira Paulista using coincidence measurements from an all-sky airglow imager, a meteor radar, and a Na temperature lidar. The event occurred between 23:42 and 01:13 local time (LT = GMT –3) and featured a prominent bright wavefront in the OH emission layer,

https://doi.org/10.5194/egusphere-2025-6569
Preprint. Discussion started: 16 February 2026

propagating from northwest to southeast (NW–SE) at an azimuthal angle of 116.6° with a phase speed of 36.7 m/s. Figure 1a shows the bright front in the OH emission at 00:27 LT. Notably, no coherent trailing wave trains followed the front, indicating a turbulent bore rather than an undular type. Concurrently, the O_2 and OI 557.7 nm airglow images (Figures 1b and 1c) revealed darkening behind the front. This intensity pattern bright in OH and dark in higher-altitude emissions suggests a vertical modulation consistent with the complementary effect described by Dewan and Picard (1998). From the images, it is possible to infer the type of mesospheric front observed, but in order to affirm such classification, analysis of the stability condition in the MLT region was done using the potential temperature (θ), (N2), (u) and (m2). Mesospheric internal bores are typically associated with ducts, which are formed due to thermal effects, Doppler effects, or a combination of both.

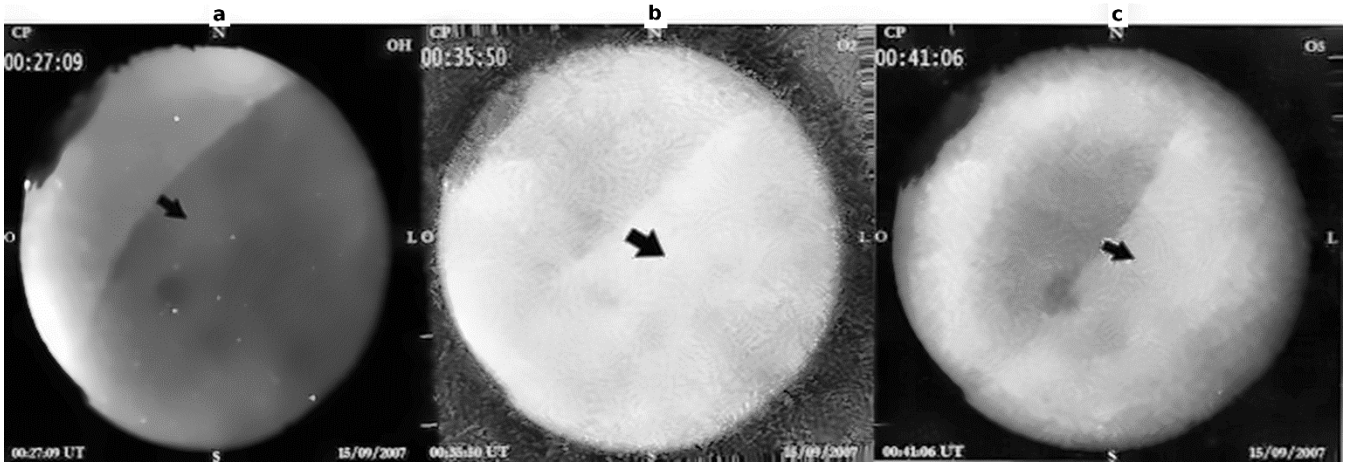

Figure 1: Airglow images of mesospheric wavefronts observed during Event 1 on the night of 14–15 September 2007. (a) A bright front in OH emission at 00:27:09 LT, (b) a corresponding dark front in O_2 (0–1) emission at 00:35:50 LT, and (c) a dark front in OI 557.7 nm (O5) emission at 00:41:06 LT. The direction of wavefront propagation is indicated by arrows in each panel.

To evaluate the background behavior of the atmospheric conditions that supported this bore, the vertical profiles from the lidar and radar at 00:30 LT (Figure 2) were examined at a time that corresponds to the bore front observation as captured across the field of view (FOV) of the all-sky imager. Panel (a) shows two temperature inversion layers (positive slopes) centered at ~87.5 km and ~97 km, suggestive of potential thermal duct formation. Panel (b) displays the N^2, indicating stable stratification. Wind profiles in panel (c) include zonal, meridional, and wave-propagation-aligned components. The error bars reflect wind retrieval uncertainties. In panel (d), m^2 profile combining wind and temperature effects shows a duct structure spanning 85–92 km, where m^2 is positive and bounded by negative values above and below, indicating a vertically trapped waveguide. To determine the dominant ducting mechanism, the contributions of temperature (Figure 2e) and wind

https://doi.org/10.5194/egusphere-2025-6569
Preprint. Discussion started: 16 February 2026

(Figure 2f) were examined separately. A strong duct structure was evident in the temperature-only profile but absent in the wind shear-only profile, indicating that the duct was primarily thermal in origin.

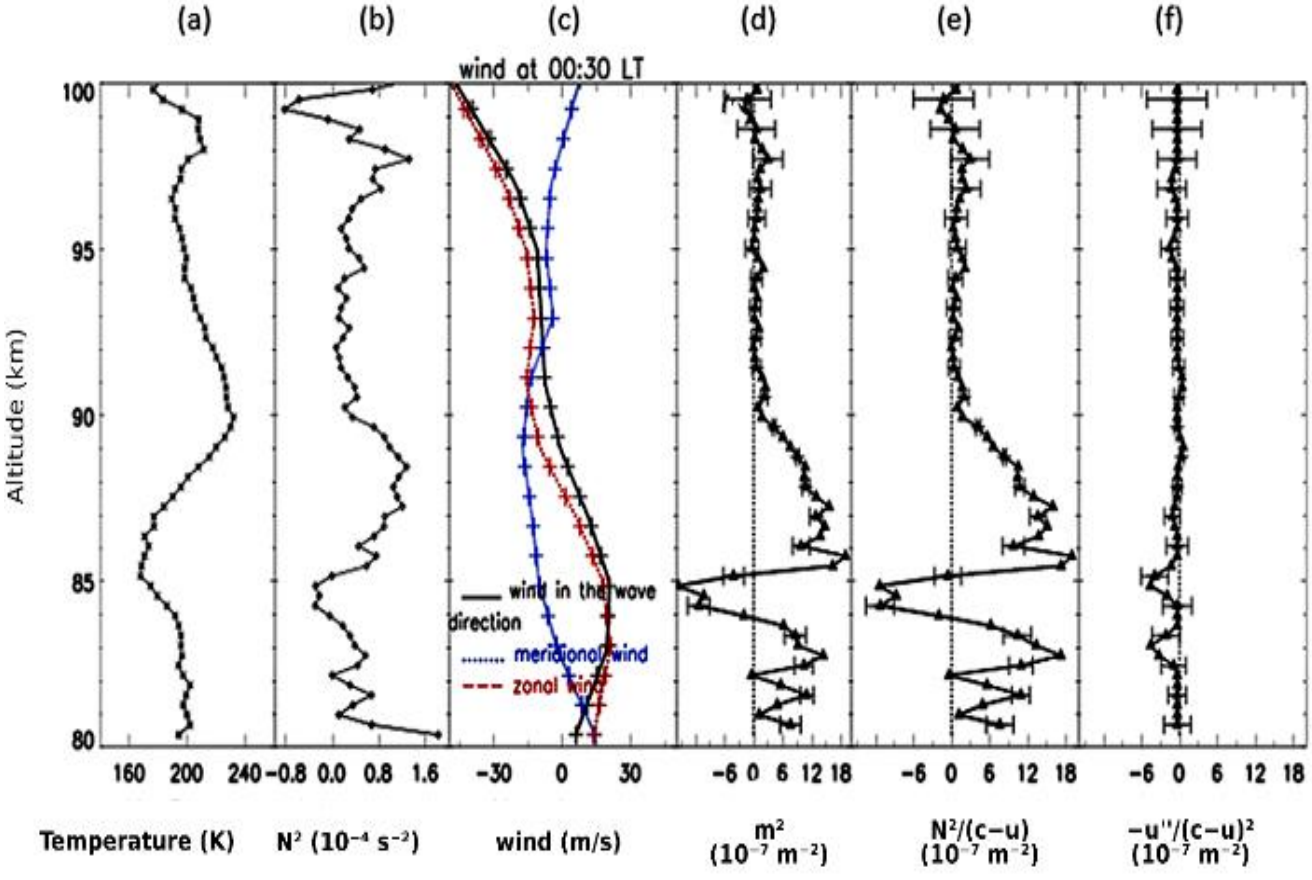

Figure 2: Vertical profiles for Event 1 on 14–15 September 2007: (a) temperature, (b) buoyancy frequency (N^2), (c) zonal, meridional, and wave-direction winds (with error bars), (d) total m^2, (e) m^2 from temperature, and (f) m^2 from wind.

The duct's vertical extent from 85–92 km overlaps with the nominal OH emission altitude (~87 km), placing the OH layer below the duct's midplane (~88.5 km). According to the complementary effect model (Dewan and Picard, 1998), such positioning results in downward compression of the OH layer, enhancing its brightness. In contrast, both the O_2 and OI emissions, located at higher altitudes (~94 km and ~97 km, respectively), lie above the duct and are expected to be pushed upward, leading to reduced emission intensity. This interpretation aligns with the observed airglow responses: a bright OH front and darkened O_2 and OI regions. Figure 3 schematically illustrates this configuration, reinforcing that the observed

https://doi.org/10.5194/egusphere-2025-6569
Preprint. Discussion started: 16 February 2026

emission pattern is consistent with the complementary effect and supports the classification of this event as a turbulent bore embedded within a thermally induced duct.

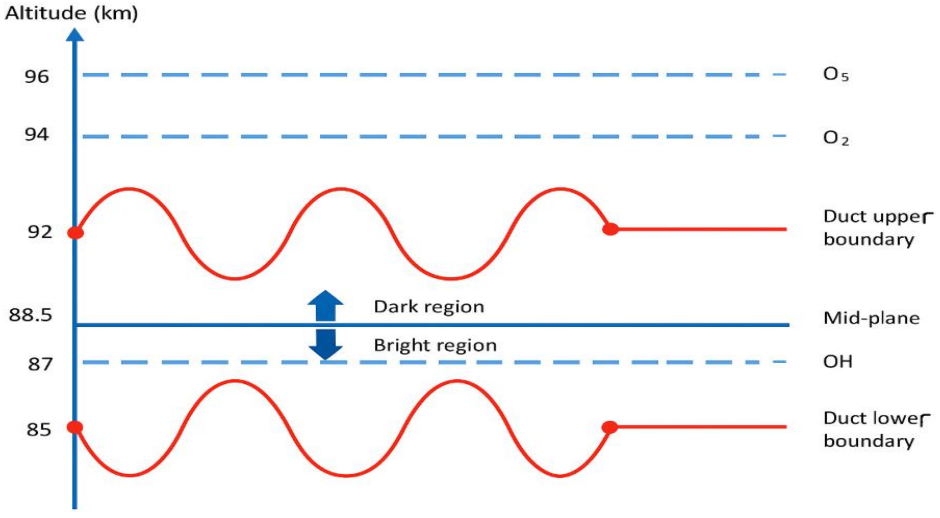

Figure 3: Schematic illustration of the oscillating duct and the resulting complementary effect on airglow emission layers at different altitudes during Event 1 (14–15 September 2007).

3.2 Event 2: 5 October 2007 — Undular Bore Driven by Thermal Ducting

On the night of 5 October 2007, a well-defined mesospheric wavefront was also observed at the same station between 20:18 and 22:11 LT using the all-sky airglow imager. The wave propagated from northwest to southeast, with an azimuth angle of 118.3° and a phase speed of approximately 54.0 m/s. The front exhibited a distinct dark leading edge in the OH airglow, followed by phase-locked trailing waves hallmarks of an undular mesospheric bore. Figure 4a shows the dark front in OH emission at 21:35:12 LT. Similar dark regions were also detected in the O_2 (Figure 4b) and OI 557.7 nm (Figure 4c) emissions, indicating a vertically coherent response across all airglow layers. This consistent dimming supports the inverse complementary effect described in literature, whereby emission layers located above a duct are displaced upward by ducted gravity waves, leading to reduced intensities.

Figure 5 shows the background conditions of the MLT region on 5 October 2007. In panel (d), a well-defined duct region is visible between 80.5 and 83 km (2.5 km), along with two other possible ducts located at 83–84.5 km and 92–94 km, respectively. Panel (e), which isolates the temperature effect, also shows a duct spanning 80.5 to 84.5 km. Additionally,

https://doi.org/10.5194/egusphere-2025-6569
Preprint. Discussion started: 16 February 2026

210 panel (f), representing the wind contribution, reveals two small duct structures: one at 86.5 - 87.5 km, and the other at 92 - 93.5 km.

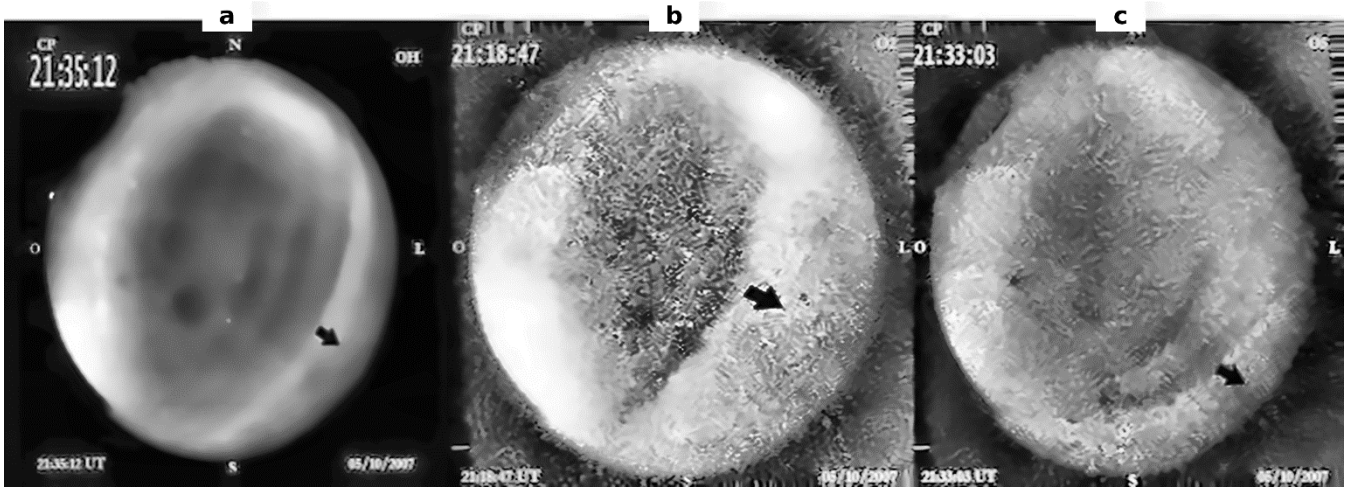

215 **Figure 4:** Airglow images of Event 2 on 5 October 2007: (a) dark front in OH at 21:35:12 LT, (b) dark front in O_2 at 21:18:47 LT, and (c) dark front in OI 557.7 nm at 21:33:03 LT. Arrows indicate the direction of propagation.

Based on the m^2 profile in panel (d), it is most likely that the wavefront propagated into the duct located between 80.5 and 220 83 km. This duct appears to have been primarily driven by the temperature structure, indicating the presence of a thermal duct rather than one induced by wind. Although another narrow propagation region was evident around 92–94 km in the m^2 profile, the observed wavefront complementary pattern does not align with propagation at that altitude. Moreover, the narrow width of this duct approximately 2.0 km is insufficient to support effective gravity wave propagation. This interpretation is further supported by the strong positional similarity between the duct seen in panel (d) and that in panel (e), 225 where a broader duct of 4.0 km extending from 80.5 to 84.5 km was observed. The greater vertical extent of this region enhances its suitability for sustaining gravity wave activity. Although some positional resemblance was also observed between panels (d) and (f), the ducts seen in panel (f) are relatively shallow less than 2.0 km thick which makes them insufficient to initiate the development of a mesospheric bore alone.

230

https://doi.org/10.5194/egusphere-2025-6569
Preprint. Discussion started: 16 February 2026

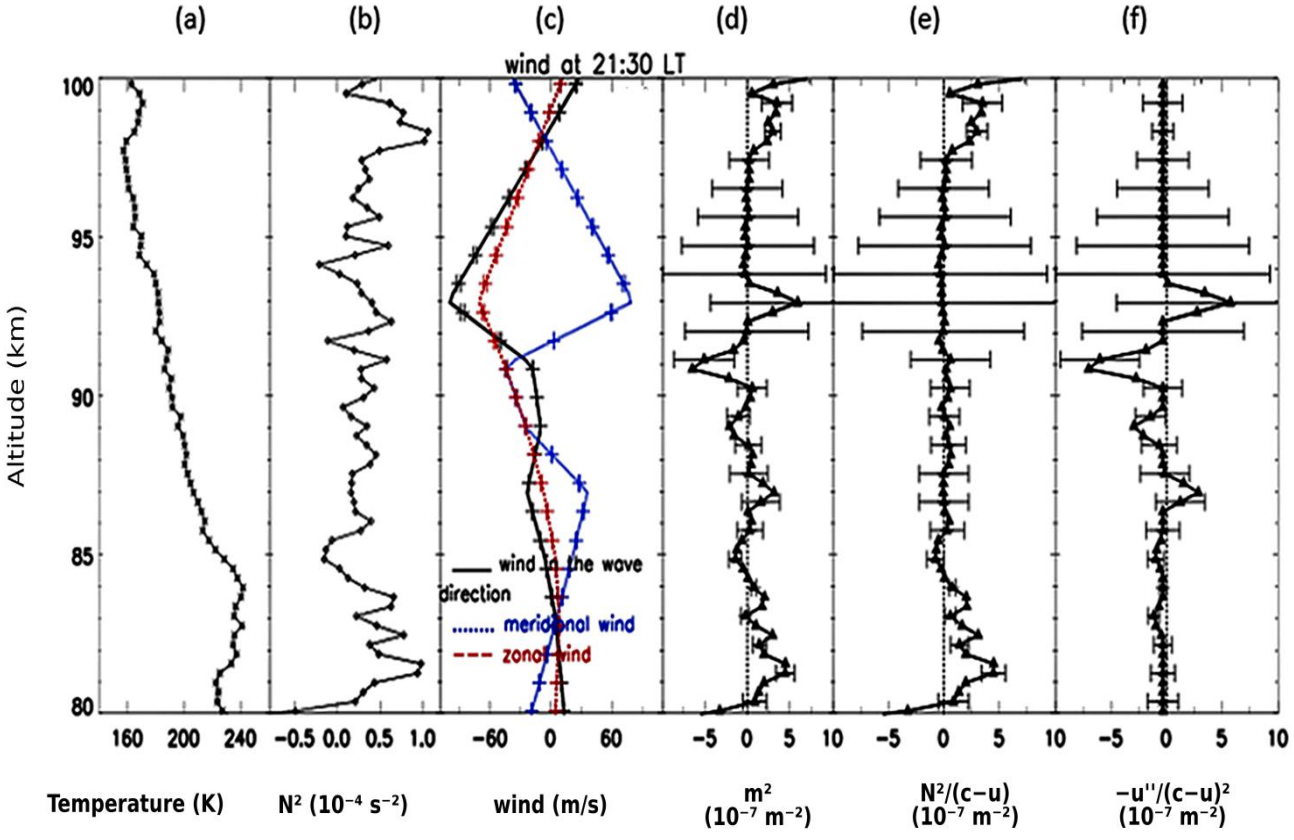

Figure 5: Vertical profiles for Event 2 (5 October 2007): (a) temperature, (b) buoyancy frequency (N^2), (c) zonal, meridional, and wave-direction winds (with error bars), (d) total m^2, (e) m^2 from temperature, and (f) m^2 from wind. The dominance of thermal inversion as the ducting mechanism supports the findings of Ramachandran et al. (2023), who showed that bore characteristics can be reproduced using thermal ducts alone.

3.3 Event 3 – 31 March 2008: Turbulent Bore Driven by a Thermal Duct

On the night of 31 March 2008, a prominent mesospheric front was captured between 21:43 and 22:57 LT. The front appeared in the OH emission as a distinct dark wavefront lacking any discernible trailing waves. It propagated from northwest to southeast (azimuth ≈ 121.6°) with a moderate phase speed of 14.7 m/s (Table 3.1). The morphology and absence of post-front wave trains are characteristic of a turbulent bore-type event. Observation time was limited due to intermittent cloud cover. Figure 6 presents the wavefront as seen across the three airglow emissions: OH, O_2 (0–1), and OI 557.7 nm. A coherent dark front is evident in all layers, maintaining a consistent propagation direction. The uniform dimming across emissions suggests that the duct responsible for the bore was located below the airglow layers, causing

https://doi.org/10.5194/egusphere-2025-6569
Preprint. Discussion started: 16 February 2026

upward vertical displacement. This resulted in reduced intensity, in agreement with the inverse complementary effect described in previous studies.

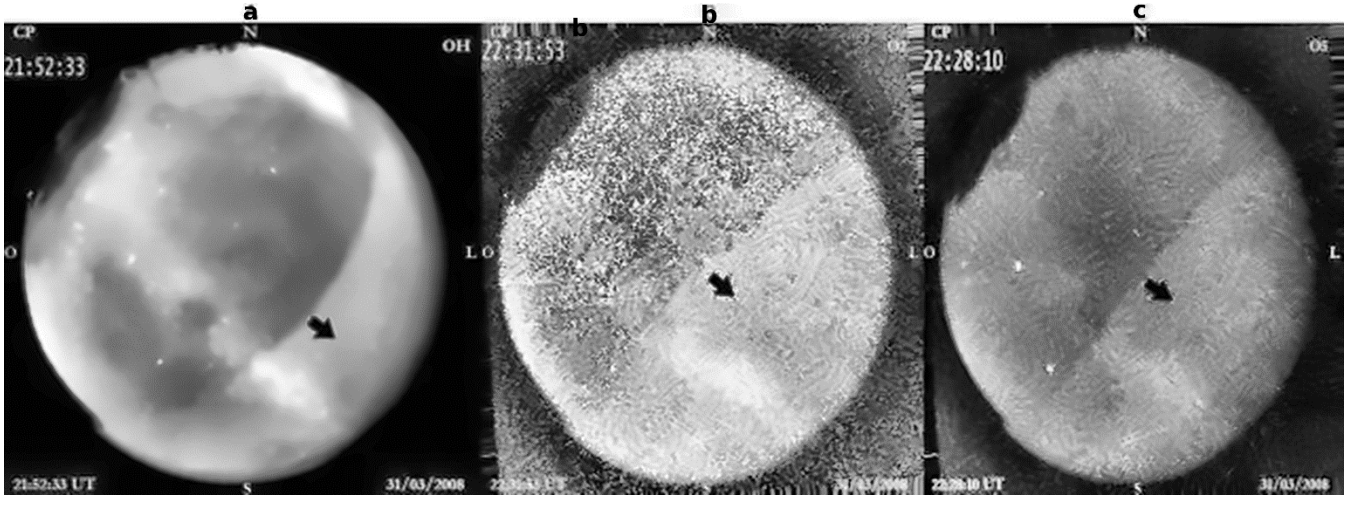

Figure 6: Airglow images of Event 4 on 31 March 2008: (a) dark front in OH emission at 21:52:33 LT, (b) dark front in O_2 emission at 22:31:53 LT, (c) dark front in OI emission at 22:28:10 LT. Arrows show the direction of propagation (azimuth ≈ 121.6°).

The vertical atmospheric profiles presented in Figure 7 further support the existence of a thermal duct between 82 and 84.5 km. The m² profile (Figure 7d) reveals a well-defined region of positive m² bounded above and below by evanescent layers, indicative of a duct capable of supporting gravity wave trapping. This duct structure is also evident in the temperature-only m² profile (Figure 7e), while the wind-only contribution (Figure 7f) shows no significant ducting features. These results suggest that the duct was primarily thermally driven, with minimal influence from wind shear. Despite the presence of a well-formed duct, the observed absence of trailing waves points to a turbulent bore regime. Such bores typically arise when incoming wave amplitudes are sufficiently large to induce wave breaking upon entering the duct, leading to enhanced energy dissipation and turbulence instead of the development of coherent trailing wave trains (Smith et al., 2005; Hecht et al., 2023).

https://doi.org/10.5194/egusphere-2025-6569
Preprint. Discussion started: 16 February 2026

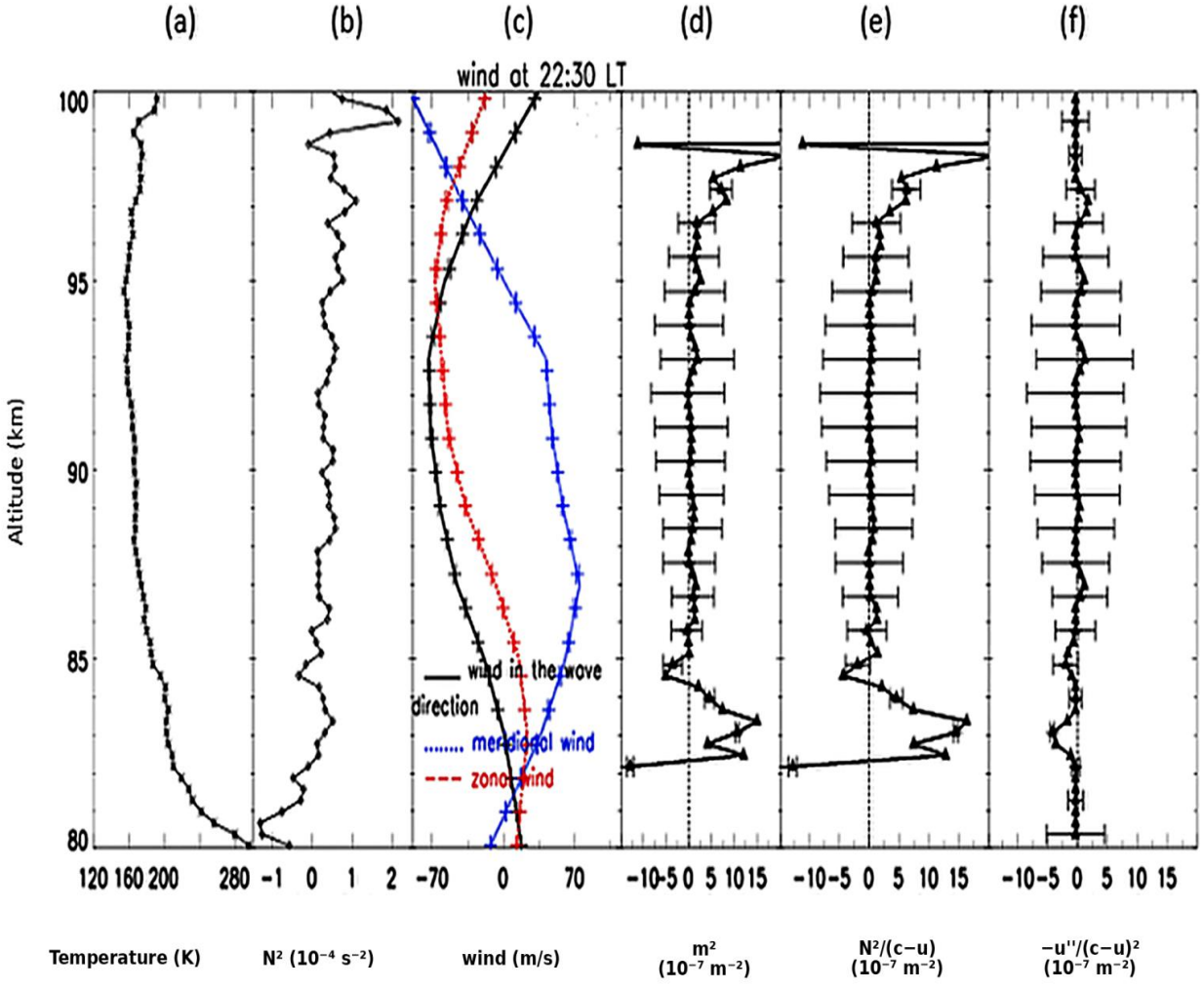

275 **Figure 7:** Vertical profiles for Event 4 on 31 March 2008: (a) temperature, (b) buoyancy frequency (N^2), (c) zonal, meridional, and wave-direction winds (with error bars), (d) total m^2, (e) m^2 from temperature, and (f) m^2 from wind.

3.4 Event 4: 3 September 2008 — Undular Bore with Multi-Duct Induced Bright Front

On the night of 3 September 2008, a distinct mesospheric front was observed between 22:21 and 23:39 LT. The
280 wave propagated from southwest to northeast (azimuth ≈ 24.8°) with a phase speed of 74.3 m/s, the highest among the four

https://doi.org/10.5194/egusphere-2025-6569
Preprint. Discussion started: 16 February 2026

events analyzed (Table 3.1). A bright leading front was recorded across all three emission layers (OH, O_2, and OI), followed by a dark trailing region (Figure 8). Notably, only a single trailing wave was phase-locked to the front unlike the typical multi-wave structure seen in classic undular bores. This morphology deviated from the classical complementary effect model, which predicts brightness variations based on the relative position of the emission layer to the duct.

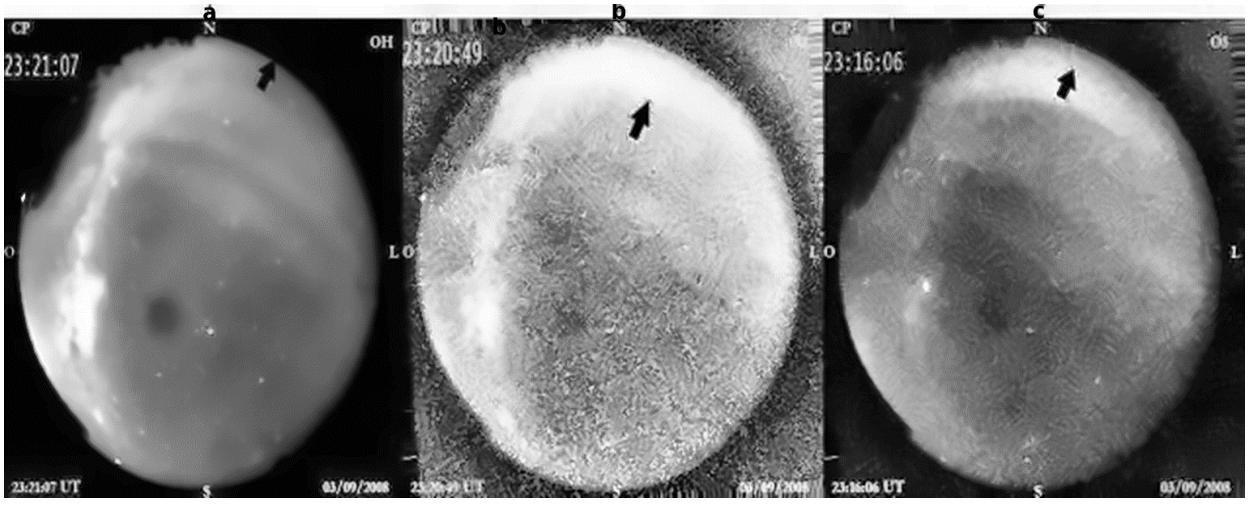

Figure 8: Airglow images of Event 5 on 3 September 2008: (a) Bright front in OH emission at 23:21:07 LT, (b) Dark front in O_2 emission at 23:20:49 LT, (c) Dark front in OI emission at 23:16:06 LT. Arrows indicate propagation direction (azimuth ≈ 24.8°).

Vertical diagnostics of the background atmosphere (Figure 9) revealed a multi-layered ducting environment. Two major ducts were identified in the m^2 profile (Figure 9d): a narrow lower thermal duct between 82 and 84.5 km, and a broader thermal-Doppler duct extending from 85 to 95.5 km. The temperature-only profile (Figure 9e) showed three duct regions at 82–84.5 km, 85–93 km, and 93.5–96 km, while the wind-only contribution (Figure 9f) revealed multiple thin Doppler ducts centered near 89, 91, and 93 km, each less than 1 km thick. This complex vertical structure suggests an interplay between thermal and wind-driven effects, with the broad upper duct overlapping typical OH and O_2 emission altitudes. The resulting wave–duct interaction led to a non-classical emission pattern: the lower thermal duct induced upward displacement, producing darkening, while the upper duct compressed the OH emission layer, enhancing brightness. This created a bright leading front followed by a dark region contrary to single-duct predictions. Although direct observations of emission responses in multi-duct settings remain limited, studies by Smith et al. (2005), Ramachandran et al. (2023) and Hecht et al. (2023), demonstrate that variations in duct characteristics strongly influence bore morphology and emission features providing reasonable analogues for interpreting complex brightness patterns in multi-layer environments demonstrating that bore morphology is sensitive to duct overlap, vertical extent, and intensity.

https://doi.org/10.5194/egusphere-2025-6569
Preprint. Discussion started: 16 February 2026

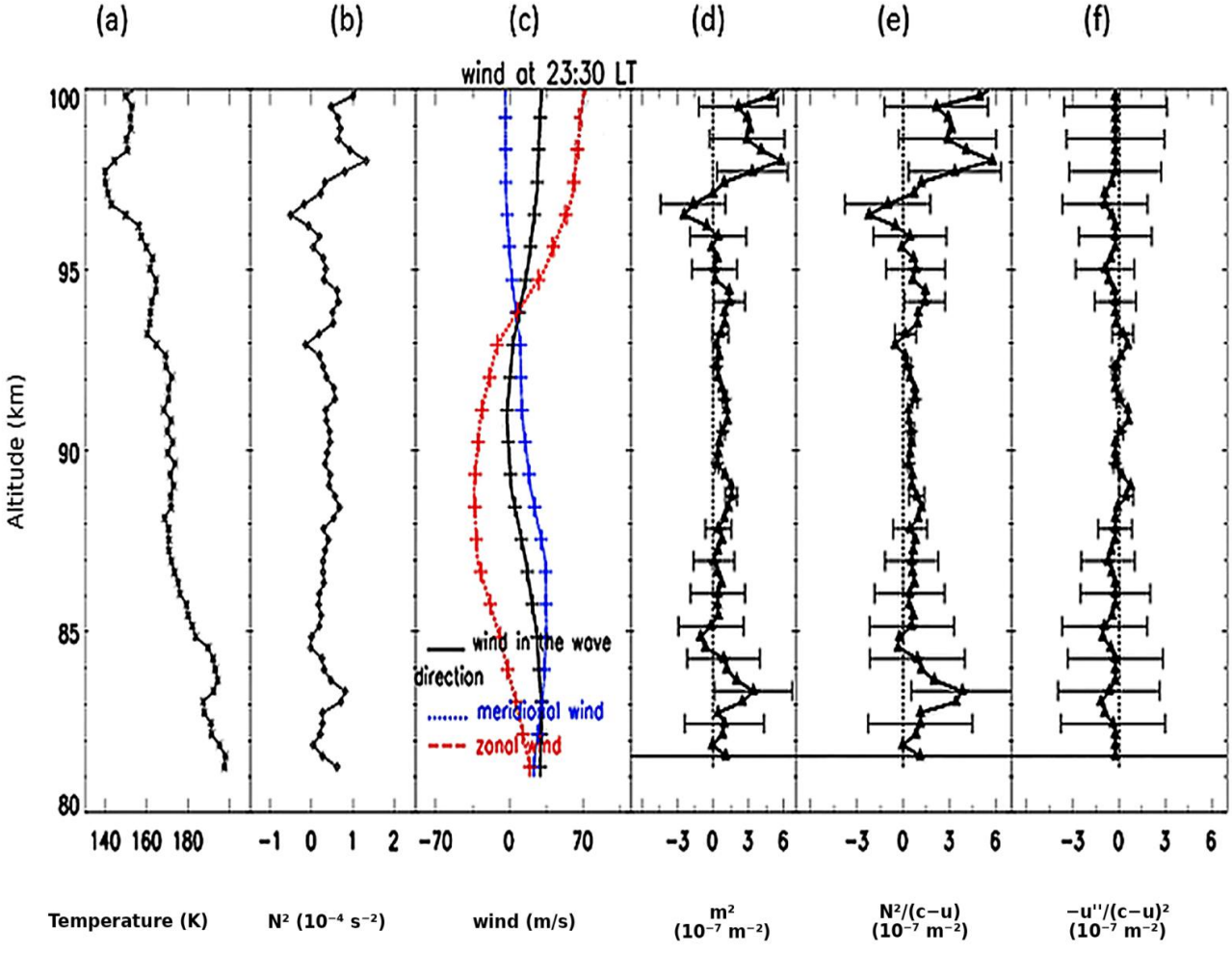

Figure 9: Vertical profiles for Event 5 on 3 September 2008: (a) temperature, (b) buoyancy frequency (N^2), (c) zonal, meridional, and wave-direction winds (with error bars), (d) total m^2, (e) m^2 from temperature, and (f) m^2 from wind.

https://doi.org/10.5194/egusphere-2025-6569
Preprint. Discussion started: 16 February 2026

4 Effects of Observed Bore Fronts

The mesospheric bore fronts analyzed in this study exhibit several important dynamical and structural impacts on the MLT. These effects are driven by the interaction of gravity waves with varying background conditions, including atmospheric ducting, wind shear, and temperature inversions. The bore-type fronts, both undular and turbulent, demonstrated significant vertical displacements of airglow layers, as evident in the alternating bright and dark bands in OH and O_2 emissions. These modulations point to strong vertical parcel motions, consistent with internal wave-induced perturbations. In cases with undular bores (Events 2), the wavefront propagated with coherent trailing wave trains, enabling efficient horizontal redistribution of energy and momentum across the ducting region. The associated vertical transport may facilitate mixing of minor species, modulate mesospheric temperature structure, and potentially impact the distribution of metallic layers such as sodium.

The turbulent bores (Events 1 and 3) lacked coherent trailing structures, instead showing signs of wave breaking and dissipation. These are indicative of localized turbulence and enhanced vertical mixing, which can modify stratification and lead to increased small-scale instability. These processes are significant for energy dissipation in the MLT and can also trigger secondary gravity wave generation or initiate Kelvin–Helmholtz instabilities during gravity wave breaking (Fritts et al., 2013).

Across all cases, the observed emission responses were consistent with theoretical expectations for wave–airglow coupling. However, multi-duct environments, such as that observed in Event 4, introduced complex brightness structures, including inversions of the typical bright/dark patterns. These observations reveal that vertical layering plays a crucial role in modulating visible signatures, with important implications for interpreting airglow imagery. They also underscore the need for collocated wind and temperature measurements to accurately infer the underlying atmospheric dynamics.

Beyond local dynamics, these mesospheric events may have significant implications for upper atmospheric interaction and signal propagation. Gravity wave-induced turbulence in the MLT can map upward into the ionosphere, leading to irregularities that cause signal scintillation and phase delays in trans-ionospheric radio transmissions, including GNSS and satellite-based communication systems. Such disturbances may degrade navigation accuracy, disrupt satellite links, and affect radar remote sensing. Moreover, enhanced momentum fluxes and localized heating from bore activity can influence ionospheric layer formation, especially under multi-duct environments.

5 Conclusion

This study provided a comprehensive, multi-instrumental analysis of four mesospheric front events observed over Cachoeira Paulista (23° S, 45° W), Brazil, between 2007 and 2008. Leveraging simultaneous observations from an all-sky airglow imager, meteor wind radar, and Na temperature lidar, the morphology of each front was characterized, their propagation dynamics were assessed, and the background MLT conditions governing their evolution were diagnosed. Among the four

https://doi.org/10.5194/egusphere-2025-6569
Preprint. Discussion started: 16 February 2026

cases, all were identified as bore-type fronts, comprising both undular and turbulent types. The classification was closely linked to the presence or absence of atmospheric ducts:

i. Thermal ducts supported Events 1, 2, and 3;
ii. Thermal-Doppler ducts enabled bore formation in Events 4;

In agreement with classical mesospheric front theory, duct width emerged as a critical parameter, with bore-supporting ducts exhibiting vertical extents of up to 10.5 km. However, direct evidence linking duct widths of ~2.5 km to significant airglow modulation is limited, studies such as Bageston et al. (2011), Giongo et al. (2018) and Ramachandran et al. (2023) demonstrate that bores in ducts just a few kilometers thick particularly thermal ducts, can substantially influence airglow intensity, trailing wave structures, and dissipative behavior. Emission responses largely adhered to the complementary effect model of Dewan and Picard (1998) in single-duct environments. However, in multi-duct scenarios (notably Event 4), classical interpretations broke down. In these cases, complex vertical layering resulted in mixed emission signatures, including the rare observation of a bright front propagating into a darkened region highlighting the importance of considering duct interaction, vertical placement, and emission altitude in future models. These findings align with numerical simulations that demonstrate how the presence of dual thermal and Doppler ducts can significantly alter bore morphology, phase structure, and energy confinement compared to single-duct scenarios (Laughman et al., 2009), Thermal gradients were identified as the dominant mechanism for duct formation, with wind shear acting synergistically in thermal-Doppler ducts. This confirms earlier hypotheses on the dual role of temperature and wind fields in establishing mesospheric trapping conditions.

Crucially, this is the first systematic mesospheric front study in Brazil's low-latitude sector employing this integrated observational framework. The coordinated use of Na lidar, meteor radar, and all-sky imaging proved essential for high-resolution vertical profiling and for resolving transient phenomena like duct transitions, emission perturbations, and front dynamics. This methodological template enhances regional and global understanding of MLT coupling processes and provides a benchmark for future research.

In summary, this study advances mesospheric front climatology by:

i. Confirming the critical role of duct width and vertical placement in front formation;
ii. Highlighting the diagnostic value of emission responses under layered ducting;
iii. Validating the influence of narrow ducts on airglow modulation;
iv. Demonstrating the necessity of multi-instrument, high-resolution datasets for mesospheric wave studies.

https://doi.org/10.5194/egusphere-2025-6569
Preprint. Discussion started: 16 February 2026

Data availability

The all-sky image, lidar and meteor radar data used to generate the results in this paper were obtained from the Observation sites da Cachoeira Paulista and São José dos Campus, which are supported by the Instituto Nacional de Pesquisas Espaciais (INPE). The data are available upon request from either Vania F. Andrioli (vania.andrioli@inpe.br), Paulo P. Batista (paulo.batista@inpe.br) or Cristiano M. Wrasse (cristiano.wrasse@inpe.br). The airglow data are available from the "Estudo e Monitoramento Brasileiro do Clima Espacial" (EMBRACE/INPE): http://www2.inpe.br/climaespacial/portal/en (EMBRACE, 20024). The TIMED/SABER data are available from https://saber.gats-inc.com/data.php (SABER, 2024).

Author contributions

EO wrote the article and performed most of the analysis. IP and VFA assisted with validation of the methodology and revision of the manuscript. PKN assisted with validation of some of the methodology and with revision of the manuscript. CMW provided the OH all-sky image data and the revision of the manuscript. PPB provided the meteor radar wind data and revised the manuscript. HT and AFM revised the manuscript.

Competing interests

The authors declare that one of the (co-)authors is a member of the editorial board of ANGEO (Igo Paulino).

Acknowledgements

The authors thank the Instituto Nacional de Pesquisas Espaciais (INPE) for providing wind and temperature data, and the Coordenação de Aperfeiçoamento de Pessoal de Nível Superior (CAPES) for financial support. I. Paulino acknowledges additional support from the Conselho Nacional de Desenvolvimento Científico e Tecnológico (CNPq) under contract 309981/2023-9. V. F. Andrioli gratefully acknowledges the China-Brazil Joint Laboratory for Space Weather, for supporting her postdoctoral fellowship.

Review statement

The review statement will be added by Copernicus Publications listing the handling editor as well as all contributing referees according to their status anonymous or identified.

https://doi.org/10.5194/egusphere-2025-6569
Preprint. Discussion started: 16 February 2026

References

Bageston, J. V., Wrasse, C. M., Hibbins, R. E., Batista, P. P., Gobbi, D., Takahashi, H., Andrioli, V. F., Fechine, J., And Denardini, C. M. (2011). Case study of a mesospheric wall event over Ferraz station, Antarctica (62° S), Ann. Geophys., 29, 209–219, https://doi.org/10.5194/angeo-29-209-2011.

Batista, P. P., Clemesha, B. R., Simonich, D. M., Taylor, M. J., Takahashi, H., Gobbi, D., Batista, I. S., Buriti, R. A., And Medeiros, A. F. (2002). Simultaneous lidar observation of a sporadic sodium layer, a "wall" event in the OH and OI5577 airglow images and the meteor winds, J. Atmos. Solar-Terr. Phys., 64, 1327–1335. DOI: 10.1016/S1364-6826(02)00116-5

Carvalho, E. B., Paulino, I., & Wrasse, C. M. (2023). A Decade of Airglow Observation of Mesospheric Fronts over the Brazilian Equatorial Region. Brazilian Journal of Geophysics, 41(2). DOI: 10.22564/brjg.v41i2.2307

Clemesha, B.R., D.M. Simonich, And P.P. Batista, (2010). Mesopause region temperature structure observed by sodium resonance lidar, J. Atmos. Sol.-Terr. Phy, 72, doi.org/10.1016/j.jastp.2010.03.017

Dewan, E., & Picard, R. (1998). Mesospheric bores. Journal Of Geophysical Research: Atmospheres, 103(D6), 6295-6305. doi: 10.1029/97jd02498

Fechine, J., Wrasse, C. M., Takahashi, H., Medeiros, A. F., Batista, P. P., Clemesha, B. R., Lima, L. M., Fritts, D., Laughman, B., Taylor, M. J., Pautet, P. D., Mlynczak, M. G., And Russell, J. M. (2009). First observation of an undular mesospheric bore in a Doppler duct, Ann. Geophys., 27, 1399–1406, https://doi.org/10.5194/angeo-27-1399-2009.

Fritts, D. C., & Wang, L. (2013). Gravity wave–fine structure interactions. Part II: Energy dissipation evolutions, statistics, and implications. *Journal of the Atmospheric Sciences*, *70*(12), 3735-3755.

Giongo, G. A., Bageston, J. V., Batista, P. P., Wrasse, C. M., Bittencourt, G. D., Paulino, I., ... & Schuch, N. J. (2018, February). Mesospheric front observations by the OH airglow imager carried out at Ferraz Station on King George Island, Antarctic Peninsula, in 2011. In *Annales Geophysicae* (Vol. 36, No. 1, pp. 253-264). Göttingen, Germany: Copernicus Publications.

Hecht, J. H., Liu, A. Z., Fritts, D. C., Walterscheid, R. L., Gelinas, L. J., & Rudy, R. J. (2023). A "boreing" night of observations of the upper mesosphere and lower thermosphere over the Andes Lidar Observatory. *Journal of Geophysical Research: Atmospheres*, *128*(20), e2023JD038754.

Hocking, W., Fuller, B., & Vandeeper, B. (2001). Real-time determination of meteor-related parameters utilizing modern digital technology. Journal Of Atmospheric And Solar-Terrestrial Physics, 63(2-3), 155-169. doi: 10.1016/s1364-6826(00)00138-3

Laughman, B., Fritts, D. C., & Werne, J. (2009). Numerical simulation of bore generation and morphology in thermal and Doppler ducts. In *Annales Geophysicae* (Vol. 27, No. 2, pp. 511-523). Copernicus GmbH.

https://doi.org/10.5194/egusphere-2025-6569
Preprint. Discussion started: 16 February 2026

Li, Q., Xu, J., Zhu, Y., Wrasse, C. M., Bageston, J. V., Yuan, W., & Liu, Z. (2025). Extreme Concentric Gravity Waves Observed in the Mesosphere and Thermosphere Regions over Southern Brazil Associated with Fast-Moving Severe Thunderstorms. *EGUsphere*, *2025*, 1-42.

Medeiros, A. F., Buriti, R. A., Machado, E. A., Takahashi, H., Batista, P. P., Gobbi, D., & Taylor, M. J. (2004). Comparison of gravity wave activity observed by airglow imaging at two different latitudes in Brazil. Journal of Atmospheric and Solar-Terrestrial Physics, 66(6-9), 647-654.

Medeiros, A., Fechine, J., Buriti, R., Takahashi, H., Wrasse, C., & Gobbi, D. (2005). Response of OH, O2 and OI5577 airglow emissions to the mesospheric bore in the equatorial region of Brazil. Advances In Space Research, 35(11), 1971-1975. doi: 10.1016/j.asr.2005.03.075

Medeiros, A., Paulino, I., Wrasse, C., Fechine, J., Takahashi, H., & Bageston, J. et al. (2018). Case study of mesospheric front dissipation observed over the northeast of Brazil. Annales Geophysicae, 36(2), 311-319. doi: 10.5194/angeo-36-311-2018

Mondal, S., Sivakandan, M., Sarkhel, S., Krishna, M. S., Mlynczak, M. G., Russell III, J. M., & Bharti, G. (2021). A case study of a thermally ducted undular mesospheric bore accompanied by ripples over the western Himalayan region. *Advances in Space Research*, *68*(3), 1425-1440.

Nappo , Carmen J.. An Introduction to Atmospheric Gravity Waves. London: Academic Press, 2002.

Narayanan, V. L., Gurubaran, S., And Emperumal, K. (2009). A case study of a mesospheric bore event observed with an all-sky airglow imager at Tirunelveli (8.7◦ N), J. Geophys. Res.-Atmos., 114, d08114, https://doi.org/10.1029/2008JD010602.

Ramachandran, K., Sivakandan, M., Chau, J. L., Urco, J. M., Gerding, M., Grundmann, S., & Smith, S. M. (2023). Investigation of a dissipating mesospheric bore using airglow imagers and direct numerical simulation. Journal of Geophysical Research: Space Physics, 128, e2022JA031114.

Simkhada, D. B., Taylor, M. J., & Franke, S. J. (2008). Doppler Ducting Measurements of Short-Period Gravity Waves and Mesospheric Bores in OH and O2 Airglow Emissions. In *AGU Fall Meeting Abstracts* (Vol. 2008, pp. SA41A-1545).

Smith, S., Friedman, J., Raizada, S., Tepley, C., Baumgardner, J., & Mendillo, M. (2005). Evidence of mesospheric bore formation from a breaking gravity wave event: simultaneous imaging and lidar measurements. Journal Of Atmospheric And Solar-Terrestrial Physics, 67(4), 345-356. doi: 10.1016/j.jastp.2004.11.008

Taylor, M., Turnbull, D., & Lowe, R. (1995). Spectrometric and imaging measurements of a spectacular gravity wave event observed during the ALOHA-93 Campaign. Geophysical Research Letters, 22(20), 2849-2852. doi: 10.1029/95gl02948

https://doi.org/10.5194/egusphere-2025-6569
Preprint. Discussion started: 16 February 2026

Wrasse, C. M., Nyassor, P. K., da Silva, L. A., Figueiredo, C. A., Bageston, J. V., Naccarato, K. P., & Gobbi, D. (2024). Studies on the propagation dynamics and source mechanism of quasi-monochromatic gravity waves observed over São Martinho da Serra (29° S, 53° W), Brazil. Atmospheric Chemistry and Physics, 24(9), 5405-5431.

Yang, G., B. Clemesha, P. Batista, And D. Simonich (2010), Seasonal variations of gravity wave activity and spectra derived from sodium temperature lidar, J. Geophys. Res., 115, D18104, doi:10.1029/2009JD012367